RoF System Based on an III-V-on-Silicon Transceiver With a Transfer-Printed PD

Zhenzhou Tang, *Student Member, IEEE*, Jing Zhang, Shilong Pan, *Senior Member, IEEE*, Gunther Roelkens, *Senior Member, IEEE*, and Dries Van Thourhout, *Member, IEEE*

***Abstract*— A full-duplex analog radio-over-fiber (RoF) system using an ultra-compact integrated III-V-on-silicon transceiver is proposed. The downstream link transmitter is realized by a 15-GHz C-band silicon ring modulator, and the upstream link receiver is constructed based on transfer printing an 11.5-GHz O-band III-V PD with a responsivity of ∼0.5 A/W. Since the transfer-printed III-V PD is transparent to the C-band downstream signal, the III-V PD is directly placed on top of the grating coupler without affecting the downstream signal, which reduces the footprint of the transceiver and also enables bidirectional transmission of the C-band and O-band signals in the same optical fiber. With the integrated transceiver, an error vector magnitude (EVM) of less than 6% is achieved for the transmission of X-band 16-QAM downstream and upstream signals with 1-Gbps data rate through a 5-km RoF link.**

***Index Terms*— Microwave photonics, silicon photonics, radio over fiber, transfer printing.**

I. Introduction

WITH the rapid increase in the wireless data traffic, next-generation wireless communication systems, 5G for example, are around the corner. They are expected to provide massive device connectivity, high system capacity and large service coverage with low latency and sustainable cost [1]. Cloud radio access networks (CRANs) are one of the key technical enablers to meet these ambitious targets, since all the remote radio heads (RRHs) are connected to a baseband unit (BBU) "pool" in the central office (CO) through low-loss optical fibers [2]. Thanks to its centralized architecture, the resources in the CO can be shared according to the traffic requirements, and the interference between the different RRHs can also be reduced by co-operative radio technologies, which enables a further increase in the density. Obviously, in the 5G wireless network, the cost, complexity and power consumption of the RRH should be reduced to relieve the budget burden due to the increasing number of connected devices. Analog radio-over-fiber (RoF) technology, due to its simple RRH structure, is regarded as one of the most convincing solutions [3]–[5]. In the analog RoF network, the analog RF signal is directly generated in the CO and transmitted to the RRH via optical fiber. The RRH only requires photodetectors (PDs) and other electronic components such as amplifiers and antennas. Expensive and usually bandwidth-limited digital-to-analog (DAC) converters and frequency conversion are thereby no more needed. Based on the analog RoF architecture, various systems have been reported, focusing mainly on pushing the carrier frequency to the millimeter-wave [6], [7] or even THz [8] band, or combining RoF with other techniques, such as massive MIMO [9], [10], and coordinated multipoint (CoMP) [11], to improve the capacity and spectral efficiency.

However, since the photonic components will be the driving force to lower the cost of the entire system, rethinking the fabrication of the photonic components is required to further reduce the costs of the RoF systems. Silicon photonics, due to its compatibility with the mature CMOS fabrication technology and its capability of manufacturing low-cost

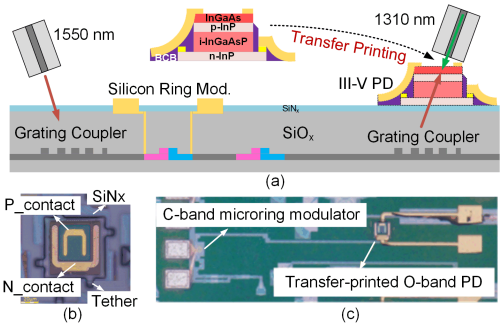

Fig. 1. (a) Cross-section of the integrated transceiver, and pictures of (b) the PD on the source wafer showing the design of the tether structure, and (c) the integrated transceiver.

Manuscript received March 28, 2019; revised May 8, 2019; accepted May 13, 2019. Date of publication May 17, 2019; date of current version June 12, 2019. This work was supported in part by the H2020 TOPHIT project, in part by the National Natural Science Foundation of China under Grant 61527820, and in part by the Fundamental Research Funds for the Central Universities. The work of Z. Tang was supported by the China Scholarship Council. (*Corresponding authors: Shilong Pan; Gunther Roelkens; Dries Van Thourhout.*)

Z. Tang is with the Photonics Research Group, Department of Information Technology, B-9052 Ghent, Belgium, also with the imec, B-3001 Leuven, Belgium, also with the Center for Nano- and Biophotonics, Ghent University, B-9000 Ghent, Belgium, and also with the Key Laboratory of Radar Imaging and Microwave Photonics, Ministry of Education, Nanjing University of Aeronautics and Astronautics, Nanjing 210016, China (e-mail: zhenzhou.tang@ugent.be).

J. Zhang, G. Roelkens, and D. Van Thourhout are with the Photonics Research Group, Department of Information Technology, B-9052 Ghent, Belgium, also with the imec, B-3001 Leuven, Belgium, and also with the Center for Nano- and Biophotonics, Ghent University, B-9000 Ghent, Belgium (e-mail: jingzhan.zhang@ugent.be; gunther.roelkens@ugent.be; dries.vanthourhout@ugent.be).

S. Pan is with the Key Laboratory of Radar Imaging and Microwave Photonics, Ministry of Education, Nanjing University of Aeronautics and Astronautics, Nanjing 210016, China (e-mail: pans@nuaa.edu.cn).

Color versions of one or more of the figures in this letter are available online at http://ieeexplore.ieee.org.

Digital Object Identifier 10.1109/LPT.2019.2917269

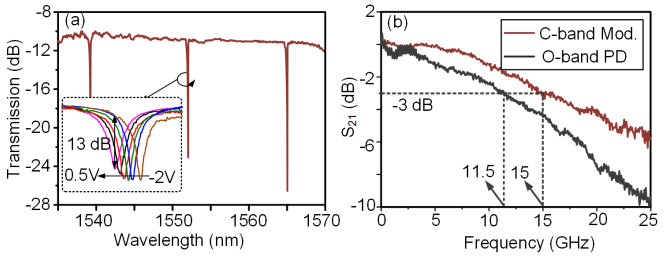

Fig. 2. Measured (a) normalized transmission response of the silicon ring modulator excluding the loss from the grating couplers, and (b) frequency responses of the ring modulator with −1 V bias and the transfer-printed PD with −3 V bias. Inset in (a): resonant wavelength shift versus bias voltage increasing from −2 V to 0.5 V with a step of 0.5 V.

devices in high volume, is very attractive for next-generation wireless communication systems. Several demonstrations, such as III-V-on-silicon lasers based on die-to-wafer bonding and Ge photodetectors (PDs) co-integrated with transimpedance amplifiers [12], [13], ring resonators for optical filtering [14], [15], GeSi parallel electro-absorption modulators (EAMs) for RF frequency upconversion [16], etc. have been reported in recent years.

Recently, we reported a novel III-V-on-silicon transceiver for a digital fiber-to-the-home (FTTH) system based on transfer printing [17]. In this Letter, with the same technology, we propose, for the first time, to the best of our knowledge, a full-duplex analog RoF system architecture utilizing wavelength division multiplexing method to enable the bidirectional signal transmission in a single optical fiber. In the proposed RoF system, electro-optic modulation of the downstream signal is realized by a C-band silicon ring modulator with a bandwidth of 15 GHz, which is integrated by the imec iSIPP25G platform. Besides, to realize the optical-to-electrical (O-E) conversion of the upstream signal, an O-band III-V PD with a responsivity of ∼0.5 A/W and a bandwidth of 11.5 GHz is transfer printed onto the same chip. Due to the 'transparency' for the C-band downstream signal of the transfer-printed O-band PD, the III-V PD is directly placed on top of the grating coupler, which makes the transceiver compact and also enables bidirectional transmission of the downstream and upstream signals in the same optical fiber without using optical circulators. An experiment based on the proposed integrated transceiver is carried out. An error vector magnitude (EVM) less than 6% is achieved in the X-band for a 1-Gbps 16QAM-modulated signal transmitted through 5-km single-mode fiber.

II. Transceiver Design and Characterization

Fig. 1(a) shows the schematic cross-section of the proposed integrated III-V-on-silicon transceiver. In the proposed transceiver, two grating couplers are integrated for the in/out coupling of light. Between the two grating couplers, a C-band silicon ring modulator for the electrical-to-optical (E-O) conversion of the downstream signal is inserted, which is fabricated in imec's iSIPP25G foundry platform. Fig. 2(a) shows the measured transmission response of the ring modulator, in which the insertion loss of the two grating couplers (8 dB in total) is excluded. The free spectral range (FSR) of the ring modulator is about 12.72 nm, and the extinction ratio is about 13 dB for a 2.5 Vpp voltage swing, as can be seen from the inset in Fig. 2(a). The electro-optic S_{21} response of the silicon modulator is also measured by an electrical vector network analyzer (Agilent N5247A) and presented in Fig. 2(b). When the ring modulator is biased at −1 V, the electro-optic modulation bandwidth of the C-band silicon ring modulator is measured to be 15 GHz.

To realize the photodetection of the upstream signal in a full-duplex RoF system, a III-V PD is integrated onto the silicon photonic circuit by transfer printing technology [18]. Transfer printing is regarded an efficient solution for the integration of III-V components realized on a III-V source substrate to a target substrate. The III-V devices can be pre-fabricated in a dense array on the source wafer and transfer-printed in a massively parallel way, which can significantly improve the material use and increase the integration throughput, thereby reducing the cost of the integration. Generally, an III-V PD is firstly fabricated on the source substrate, which contains a 1-μm thick InGaAsP absorbing layer to push the cut-off wavelength of the PD to 1.37 μm (i.e., O-band). Then, the PD is encapsulated by a 2.5-μm thick photoresist layer with narrow tethers (as shown in Fig. 1(b)), and wet etching is used to etch the release layer (1 μm thick InGaAs) and undercut the pre-fabricated PD. Finally, a PDMS stamp is used to pick-up and print the III-V PD to the target substrate (SOI in this letter) by an X-Celeprint μTP-100 tool. The detailed process flow can be found in our previous publication [17]. The responsivity of the PD is about 0.5 A/W at −3 V bias, which is 4 orders of magnitude higher than that at the C-band. Since the PD is 'transparent' for the C-band downstream signal, it is directly placed onto the grating coupler to make the transceiver compact and also guarantee the bidirectional signal transmission through the same optical fiber without using optical circulators, as can be seen from Fig. 1(c). The measured 3-dB bandwidth of the O-band PD is 11.5 GHz, which is shown in Fig. 2(b) as well.

III. Experiment and Results

With the integrated transceiver an experiment based on the scheme shown in Fig. 3 is carried out. In the CO, 12-dBm continuous wave (CW) light is generated by a C-band tunable laser source (Santec TSL-510) and coupled into the C-band silicon ring modulator via a polarization controller (PC). According to the transmission response of the ring modulator shown in Fig. 2, the wavelength of the optical carrier is chosen to be 1552.128 nm to ensure sufficient E-O modulation efficiency. For the downstream link, the RF signal applied to the ring modulator is 16QAM data at a 10 GHz carrier frequency with a data rate of 0.2 and 1 Gb/s (i.e., 50 and 250-Mbaud), which is generated by an arbitrary waveform generator (Keysight M9052A). The bias for the ring modulator is −0.7 V, which is generated by a DC source (Keithley 2401) and applied through a bias tee. The modulated optical downstream signal is then coupled out via another grating coupler and the transfer-printed O-band PD on top of it. Through 5-km single-mode fiber link, the downstream signal

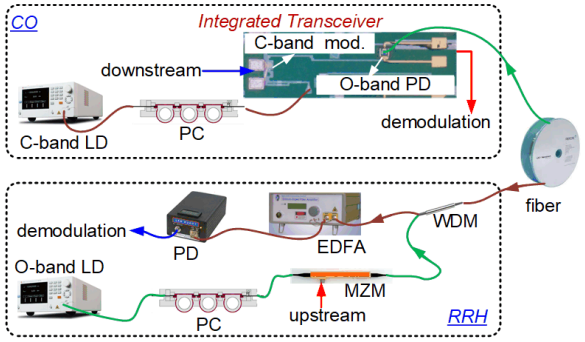

Fig. 3. Schematic diagram of the full-duplex analog RoF system based on the integrated transceiver.

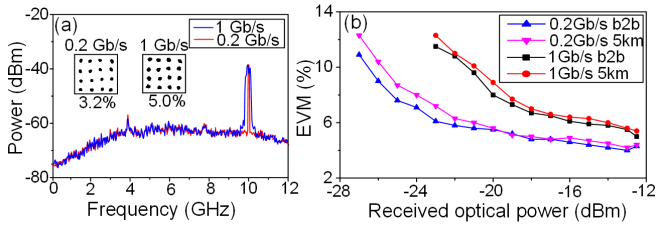

Fig. 4. Measured (a) electrical spectra of the 0.2- and 1-Gb/s downstream signals and (b) EVM versus received optical power for back-to-back (b2b) and 5-km downstream link. Inset: Constellation diagrams of the demodulated 0.2- and 1-Gb/s 16QAM data.

is transmitted to a RRH. In the RRH, the downstream signal is boosted by an erbium-doped fiber amplifier (EDFA) and sent to a commercially-available PD with a bandwidth of 20 GHz and a responsivity of ∼0.7 A/W. The recovered electrical signal is sent to a 13.6-GHz electrical spectrum analyzer (R&S FSP13) and one channel of a 63-GHz real-time oscilloscope (Keysight DSA-Z 634A) to realize electrical spectrum analysis and QAM signal demodulation, respectively.

For the upstream link, 5-dBm CW light with a wavelength of 1356 nm is generated by an O-band tunable laser source (Santec TSL-510) and sent to an O-band modulator via another PC. The upstream signal, 50 and 250-Mbaud 16QAM data with a carrier frequency of 8 GHz, is generated by another channel of the AWG. The modulated O-band upstream optical signal is duplexed with the C-band downstream signal by a wavelength division multiplexer (WDM) and transmitted back to the CO through the same 5-km optical fiber without using optical circulators. In the CO, the upstream signal is detected by the transfer-printed O-band III-V PD. The electrical signal obtained by the O-band PD is also sent to the electrical spectrum analyzer and another channel of the real-time oscilloscope for the electrical spectrum measurement and QAM data demodulation, respectively.

Fig. 4(a) shows the measured electrical spectra of the 10-GHz band 0.2- and 1-Gb/s 16QAM downstream signals at the output of the PD in the RRH, when the optical power applied to the PD is about 0.5 dBm. The corresponding constellation diagrams are also shown as insets in Fig. 4(a), and have an EVM of 3.2 % and 5%, respectively. Fig. 4(b) shows the measured relationship between the EVM and the received optical power for the downstream link. As can be seen, when the received optical power is > -22 dBm, the EVM is $<6\%$,

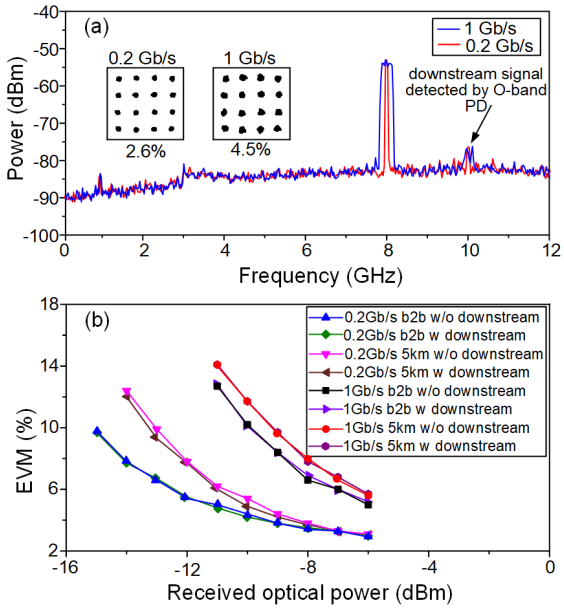

Fig. 5. Measured (a) electrical spectra of the 0.2- and 1-Gb/s upstream signals and (b) EVM versus received optical power for b2b and 5-km upstream link with the downstream link switched on or off. Inset: Constellation diagrams of the demodulated 16QAM data.

for the transmission of the 0.2-Gb/s 16QAM data. When the downstream signal is a 1-Gb/s 16QAM data, the EVM is $<6\%$ if the received optical power is > -15 dBm. In addition, the impact of the 5-km fiber link on the downstream transmission is limited due to its low fiber transmission loss in the C-band and also the low fiber dispersion distortion for the X-band RF signal transmission.

Similarly, Fig. 5(a) shows the measured spectra of the 8-GHz band, 0.2- and 1-Gb/s 16QAM upstream signal, when -4.6 dBm optical power is applied to the transfer-printed O-band PD in the CO. The corresponding constellation diagrams, with EVMs of 2.6% and 4.5%, are presented as the insets. In Fig. 5(b), the measured EVM as a function of the received optical power for the upstream link is depicted. As can be seen, when the date-rate of the upstream signal is 0.2 Gb/s, the EVM, after 5-km fiber transmission, is lower than 6%, if the received optical power is higher than -11 dBm. When the date-rate of the upstream signal is increased to 1-Gb/s, an EVM of $<6\%$ is obtained when the received optical power is > -6 dBm. As compared with the back-to-back (b2b) transmission, the 5-km fiber transmission link introduces a slight deterioration in the EVM, which may result from the relatively higher fiber transmission loss in the O-band. Besides, to check the crosstalk between the C-band downstream and O-band upstream signal in the O-band PD, the EVMs with and without downstream signal transmission are also compared and no obvious change is observed according to the results in Fig. 5(b).

Fig. 6(a) shows the spurious free dynamic range (SFDR) of the 10-GHz downstream link when the bias voltage of the ring modulator is -1 V. With a measured noise floor of -150 dBm, the SFDR is about 82 dB $\cdot$ $Hz^{2/3}$. Fig. 6(b) presents the SFDR with different bias voltages of the ring modulator. The measured SFDR is within 81 $\sim$ 84 dB $\cdot$ $Hz^{2/3}$ when the bias

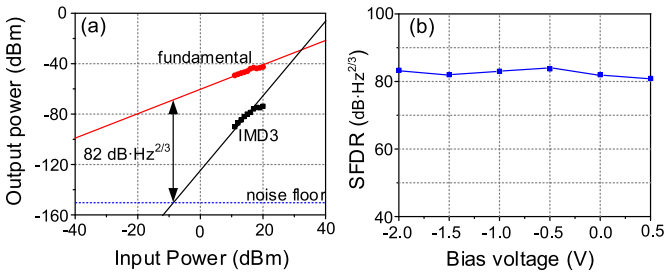

Fig. 6. (a) Measured spurious free dynamic range (SFDR) of the 10-GHz downstream link when the bias voltage of the ring modulator is −1 V, and (b) the SFDR versus the bias voltages of the ring modulator.

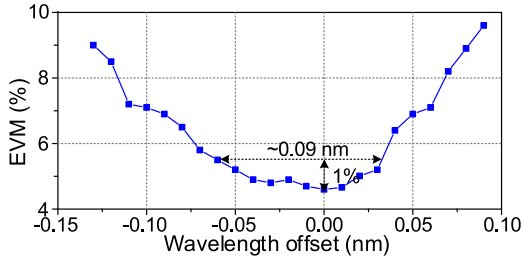

Fig. 7. Measured EVM versus the wavelength offset.

voltage is tuning from 0.5 to −2 V. In addition, to investigate the transmission performance dependence on the wavelength of the optical carrier, EVM of the 0.2-Gb/s 16QAM data versus the optical carrier wavelength offset is measured and shown in Fig. 7. As can be seen, the EVM is increased by 1 % when the wavelength drift is from −0.06 to 0.03 nm. As a result, to ensure the best transmission performance, feedback loop for the wavelength tracking and locking is desired [18].

Since the 3-dB bandwidths of the ring modulator and the transfer-printed PD are 15 and 11.5 GHz, the proposed full-duplex RoF link is designed to work in the X-band. However, if the ring modulator would be realized in imec's newest iSIPP50G platform and a modified design is employed for the PD, the bandwidth of the transceiver can be largely increased, enabling millimeter-wave RoF systems. Furthermore, transfer printing has the advantage of parallel device pick-up and print, so multichannel transceivers would be possible [19], which can further increase the capacity, if wavelength division multiplexing technology is also employed. The laser and PC are still off chip due to the lack of laser source on silicon materials. Fortunately, this issue can be solved by using transfer printing technology as well [20], so a fully-integrated transceiver consisting of a transfer-printed LD, a silicon modulator and a transfer-printed PD is expectable in the near future.

IV. Conclusion

In this letter, we have demonstrated an X-band full-duplex analog RoF system based on an integrated III-V-on-silicon transceiver. The downstream signal is imprinted on a C-band optical carrier through a 15-GHz C-band silicon ring modulator, and the photodetection of the upstream signal is implemented by the integration of a 11.5-GHz O-band III-V PD using transfer printing. Error-free transmission (EVM < 6%) for both the downstream and upstream links is achieved without using optical circulators. The work shows the great potential of transfer printing for the integration of III-V-on-silicon devices, so we believe that silicon photonics together with transfer printing is a promising technology for low-cost and high-throughput integration of optical devices, which may offer improved performance, reduced cost and increased functionality in future wireless communication systems.

References

[1] A. Gupta and E. R. K. Jha, "A survey of 5G network: Architecture and emerging technologies," *IEEE Access*, vol. 3, pp. 1206–1232, 2015.
[2] *C-RAN: The Road Towards Green RAN*, China Mobile Res. Inst., Beijing, China, 2013.
[3] Z. Z. Tang and S. L. Pan, "A full-duplex radio-over-fiber link based on a dual-polarization Mach—Zehnder modulator," *IEEE Photon. Technol. Lett.*, vol. 28, no. 8, pp. 852–855, Apr. 15, 2016.
[4] Z. Cao *et al.*, "Energy efficient and transparent platform for optical wireless networks based on reverse modulation," *IEEE J. Sel. Areas Commun.*, vol. 31, no. 12, pp. 804–814, Dec. 2013.
[5] C. Lim, A. Nirmalathas, K. L. Lee, D. Novak, and R. Waterhouse, "Inter-modulation distortion improvement for fiber-radio applications incorporating OSSB+C modulation in an optical integrated-access environment," *J. Lightw. Technol.*, vol. 25, no. 6, pp. 1602–1612, Jun. 1, 2007.
[6] J. V. Kerrebrouck *et al.*, "10 Gb/s radio-over-fiber at 28 GHz carrier frequency link based on 1550 nm VCSEL chirp enhanced intensity modulation after 2 km fiber," in *Proc. Opt. Fiber Commun. Conf. Expo. (OFC)*, Mar. 2018, pp. 1–3.
[7] Z. Z. Tang, F. Z. Zhang, and S. L. Pan, "60-GHz RoF system for dispersion-free transmission of HD and multi-band 16 QAM," *IEEE Photon. Technol. Lett.*, vol. 30, no. 14, pp. 1305–1308, Jul. 15, 2018.
[8] X. Y. Li *et al.*, "120 Gb/s wireless terahertz-wave signal delivery by 375 GHz-500 GHz multi-carrier in a 2Ã–2 MIMO system," in *Proc. Opt. Fiber Commun. Conf. Expo. (OFC)*, Mar. 2018, pp. 1–3.
[9] L. Cheng, X. Liu, N. Chard, F. Effenberger, and G. Chang, "Experimental demonstration of sub-Nyquist sampling for bandwidth- and hardware-efficient mobile fronthaul supporting 128×128 MIMO with 100-MHz OFDM signals," in *Proc. Opt. Fiber Commun. Conf. Expo. (OFC)*, Mar. 2016, pp. 1–3.
[10] U. Habib, A. E. Aighobahi, T. Quinlan, S. D. Walker, and N. J. Gomes, "Analog radio-over-fiber supported increased RAU spacing for 60 GHz distributed MIMO employing spatial diversity and multiplexing," *J. Lightw. Technol.*, vol. 36, no. 19, pp. 4354–4360, Oct. 1, 2018.
[11] Y. Tian, K. L. Lee, C. Lim, and A. Nirmalathas, "Performance evaluation of CoMP for downlink 60-GHz radio-over-fiber fronthaul," in *Proc. Int. Top. Meeting Microw. Photon. (MWP)*, Oct. 2017, pp. 1–4.
[12] K. V. Gasse *et al.*, "Analog radio-over-fiber transceivers based on III-V-on-silicon photonics," *IEEE Photon. Technol. Lett.*, vol. 30, no. 21, pp. 1818–1821, Nov. 1, 2018.
[13] K. V. Gasse *et al.*, "III-V-on-silicon photonic transceivers for radio-over-fiber links," *J. Lightw. Technol.*, vol. 36, no. 19, pp. 4438–4444, Oct. 1, 2018.
[14] M. H. Huang, S. M. Li, M. Xue, L. Zhao, and S. L. Pan, "Flat-top optical resonance in a single-ring resonator based on manipulation of fast-and slow-light effects," *Opt. Express*, vol. 26, no. 18, pp. 23215–23220, Sep. 2018.
[15] C. L. Manganelli *et al.*, "Large-FSR thermally tunable double-ring filters for WDM applications in silicon photonics," *IEEE Photon. J.*, vol. 9, no. 1, pp. 1–10, Feb. 2017.
[16] K. V. Gasse, J. Verbist, H. Li, G. Torfs, J. Bauwelinck, and G. Roelkens, "Silicon photonics radio-over-fiber transmitter using GeSi EAMs for frequency up-conversion," *IEEE Photon. Technol. Lett.*, vol. 31, no. 2, pp. 181–184, Jan. 15, 2019.
[17] J. Zhang *et al.*, "Silicon photonics fiber-to-the-home transceiver array based on transfer-printing-based integration of III-V photodetectors," *Opt. Express*, vol. 25, no. 13, pp. 14290–14299, Jun. 2017.
[18] S. Agarwal, M. Ingels, M. Pantouvaki, M. Steyaert, P. Absil, and J. V. Campenhout, "Wavelength locking of a Si ring modulator using an integrated drop-port OMA monitoring circuit," *IEEE J. Solid-State Circuits*, vol. 51, no. 10, pp. 2328–2344, Oct. 2016.
[19] B. Corbett, R. Loi, J. O'Callaghan, and G. Roelkens, "Transfer printing for silicon photonics," *Semicond. Semimet.*, vol. 99, pp. 43–70, May 2018.
[20] J. Zhang *et al.*, "Transfer-printing-based integration of a III-V-on-silicon distributed feedback laser," *Opt. Express*, vol. 26, no. 7, pp. 8821–8830, Apr. 2018.